Hybrid analytical / numerical coupled-mode modeling of guided wave devices

Manfred Hammer,

MESA$^+$ Institute for Nanotechnology, University of Twente, Enschede, The Netherlands,

Abstract: A general version of coupled-mode-theory for frequency domain scattering problems in integrated optics is proposed. As a prerequisite a physically reasonable field template is required, that typically combines modes of the optical channels in the structure with coefficient functions of in principle arbitrary coordinates. Upon 1-D discretizations of these amplitude functions into finite elements, a Galerkin procedure reduces the problem to a system of linear equations in the element coefficients, where given input amplitudes are included. Smooth approximate solutions are obtained by solving the system in a least squares sense. The versatility of the approach is illustrated by means of a series of 2-D examples, including a perpendicular crossing of waveguides, and a grating-assisted rectangular resonator. As an appendix, we show that alternatively a similar procedure can be derived by variational means, i.e. by restricting a suitable functional representation of the full 2-D/3-D vectorial scattering problem (with transparent influx boundary conditions for inhomogeneous exterior) to the respective field templates.
Keywords: integrated optics, numerical modeling, coupled mode theory, variational modeling, transparent influx boundary conditions.

PACS codes: 42.82.–m 42.82.Bq 42.82.Et

1 Introduction

Frequently, the propagation of light through integrated optical structures is discussed in terms of interactions of a few known basis fields, typically the guided modes that are supported by the local optical channels of the device. Up to some remainder it is then usually straightforward to write a reasonable ansatz for the optical field by superimposing the respective basis fields with coefficient functions that vary along the associated propagation coordinate. One obtains — necessarily approximate — equations for the amplitudes of the basis fields, and their solutions. Approaches of this kind are usually addressed by the term "coupled mode theory" (CMT); we refer to Refs. [1, 2] and to the papers included in the SPIE Milestones Series volume [3] for overviews. For the fundamental case of evanescent interaction of guided light waves in parallel, longitudinally homogeneous dielectric channels, Ref. [4] gives a derivation of the coupled mode equations by variational means. Only in special situations — typically for longitudinally homogeneous systems of few waveguides — the CMT equations permit analytical solutions, i.e. lead to explicit analytical expressions that describe the light propagation. For other, by no means less interesting configurations one obtains e.g. coupled systems of differential equations of higher dimension, or systems with non-constant coefficients, that can only be treated by numerical means. Then the solutions consist of numerical representations of the CMT coefficient functions, that still permit to inspect the amplitude evolutions. The term "CMT" is used here in a way that encompasses explicitly these situations.

The collection of "selected papers on coupled-mode theory in guided-wave optics" [3] classifies the existing methods for linear structures by the terms "codirectional" CMT, covering the codirectional propagation of modes along closely spaced, more or less parallel waveguide cores, and "contradirectional" CMT, which is concerned with the wave propagation in corrugated channels (waveguide gratings). All techniques rely on the introduction of a common propagation coordinate, which appears to be decidedly unnatural, e.g. in the case of optical microring resonators coupled to straight waveguides [5, 6, 7]. Light propagation is modeled from a viewpoint of the evolution of mode amplitudes along this propagation coordinate. Sets of coupled ordinary differential equations are established for the mode amplitudes and solved by analytical or numerical means. One also sees the approach frequently used as a phenomenological model, where certain quantities in the equations are not rigorously linked to the Maxwell equations, to the basis fields the interaction of which is discussed, and to the underlying structure, i.e. coupling coefficients are treated as fit-parameters.

* *Department of Applied Mathematics, University of Twente P.O. Box 217, 7500 AE Enschede, The Netherlands*
Phone: +31/53/489-3448 Fax: +31/53/489-4833 E-mail: m.hammer@math.utwente.nl

We shall see that the above classification is unnecessary for the approach proposed in this paper. The unified formalism covers co- and contradirectional propagation, where applicable. Moreover, a common propagation coordinate is not required; the technique can be applied even to a structure with modes traveling along perpendicularly oriented channels. Starting from first principles, i.e. with the frequency domain Maxwell equations, once a physically plausible field template has been fixed for a given structure, no further heuristics is required to arrive at the desired approximate solutions for the optical field.

Section 2 outlines the underlying theory. Given the geometry and refractive index profile of a dielectric circuit, first a reasonable ansatz for the electromagnetic fields has to be fixed. Typically the expressions incorporate the guided modes (profiles and exponential terms) that are supported locally by the channels in the structure. These are multiplied by amplitude functions which depend on the propagation coordinate that is most convenient for the respective mode. Then what remains is to determine the strength of the interactions, i.e. to determine the amplitude functions. Here we use numerics: the amplitude functions are discretized by linear 1-D finite elements (FE). A Galerkin procedure permits to establish a dense, but small-size system of linear equations for the element coefficients, which is finally solved numerically.

In Section 3, the theory is applied to a series of 2-D examples, where either analytical or numerical results are available for comparison. At hand of the perpendicular waveguide crossing, which already serves to introduce the theory in Section 2, we show that it is also possible — with limitations — to incorporate radiation losses by suitable field templates, e.g. by properly placed Gaussian beams. One should be aware that in general the range of applicability of CMT approaches need not be restricted to structures with “low” refractive index contrast. The examples in e.g. Refs. [8, 6, 7] and also in this paper cover structures with moderate to high index contrast, but with only relatively weak, or only localized mutual perturbations of the interacting basis modes, such that the optical fields can well be described by the CMT templates.

The Galerkin projection introduced in Section 2 naturally raises the question whether the formalism can be derived alternatively by variational means [1]. Also to give some motivation why the former procedure is applied in the way described, in the appendix we show that this is indeed possible. The reasoning starts with a functional of the six electromagnetic field components. If this functional becomes stationary, its arguments satisfy the Maxwell equations in the domain of interest, together with suitable conditions (transparent influx boundary conditions, cf. e.g. Refs. [9, 10, 11]) on the input / output “ports” that constitute its boundary. Upon restricting the functional to the FE coefficients of the amplitude functions in the CMT field template, a linear system of equations for these unknowns is obtained by requiring the restricted functional to become stationary. At least for the example of the waveguide crossing, the alternative formalism can reproduce the results of Section 3. At the same time the approach of Section 2 has certain practical advantages when compared with the alternative formalism. The appendix closes with respective comments.

2 Theory

Figure 1 introduces a 2-D example structure along which the “hybrid” CMT approach (HCMT) will be explained. Adaptation for other types of structures should be straightforward. Also we adopt a notation that permits a straightforward extension to three spatial dimensions. Frequency domain equations are considered, i.e. the optical fields are meant to vary harmonically in time $\sim \exp(\mathrm{i}\omega t)$ with angular frequency $\omega = 2\pi\mathrm{c}/\lambda$, always specified by the vacuum wavelength λ, for vacuum speed of light c.

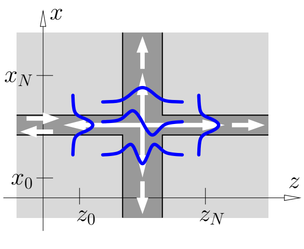

Figure 1: A perpendicular crossing of two waveguide cores, described in Cartesian coordinates x, z. The region of interest is enclosed by a computational window $x \in [x_0, x_N]$, $z \in [z_0, z_N]$. Bidirectional versions of the guided modes supported by the two channels serve as basis fields for the CMT model.

In the 2-D case, the structure and all fields are assumed to be constant in the y-direction; derivatives with respect to y that appear e.g. in the curl operators in Eqs. (6) vanish, integrals with respect to y as in Eq. (17) should be omitted. By writing things out in components, in 2-D the entire formulation below can be split in separate expressions for TE and TM polarized fields, just as the Maxwell equations (6). Basis modes (1) are then the familiar TE- and TM-modes of multilayer slab waveguides with 1-D cross sections, given in terms of a scalar principal electric (TE) or magnetic component (TM). Other field components are derived from these principal profiles, as required for the formalisms of Section 2.3 and Section A.2.

2.1 Coupled mode field template

A plausible and convenient template for the electromagnetic fields forms the starting point for the further CMT analysis. In case of the waveguide crossing of Figure 1 being illuminated from the left via a guided mode of the horizontal channel, one expects the following behaviour: Upon entering the region where the waveguides meet, the incoming wave will transfer parts of its power to other modes of the horizontal core that also run from left to right, to modes of the horizontal channel that propagate from right to left, and to modes supported by the vertical waveguide that travel upward or downward. Another part of the optical power will leave the crossing region in the form of nonguided waves, where for the moment we assume that this last part can be neglected.

Hence the guided modes associated with the two waveguides are the principal constituents for the CMT field template. These are of the form

$$\boldsymbol{\psi}_m^{\mathrm{f,\,b}}(x,z) = \begin{pmatrix} \tilde{\boldsymbol{E}} \\ \tilde{\boldsymbol{H}} \end{pmatrix}_m^{\mathrm{f,\,b}}(x)\ \mathrm{e}^{\mp\mathrm{i}\beta_m^{\mathrm{h}} z} \quad \text{and} \quad \boldsymbol{\psi}_n^{\mathrm{u,\,d}}(x,z) = \begin{pmatrix} \tilde{\boldsymbol{E}} \\ \tilde{\boldsymbol{H}} \end{pmatrix}_n^{\mathrm{u,\,d}}(z)\ \mathrm{e}^{\mp\mathrm{i}\beta_n^{\mathrm{v}} x}. \tag{1}$$

Here upper indices f,b identify either the forward or backward propagating version of the mode of order m of the horizontal core with electric part $\tilde{\boldsymbol{E}}_m^{\mathrm{f,b}}$ and magnetic part $\tilde{\boldsymbol{H}}_m^{\mathrm{f,b}}$ of the mode profile, functions of the transverse coordinate x, corresponding to exponential dependences on the propagation coordinate z with propagation constant $\mp\beta_m^{\mathrm{h}}$. Analogously, indices u, d denote the upward or downward traveling modes of the vertical waveguide, with propagation constants $\mp\beta_n^{\mathrm{v}}$.

Thus a reasonable field template for the waveguide crossing reads

$$\begin{aligned} \begin{pmatrix} \boldsymbol{E} \\ \boldsymbol{H} \end{pmatrix}(x,z) &= \sum_m f_m(z)\,\boldsymbol{\psi}_m^{\mathrm{f}}(x,z) + \sum_m b_m(z)\,\boldsymbol{\psi}_m^{\mathrm{b}}(x,z) \\ &+ \sum_n u_n(x)\,\boldsymbol{\psi}_n^{\mathrm{u}}(x,z) + \sum_n d_n(x)\,\boldsymbol{\psi}_n^{\mathrm{d}}(x,z), \end{aligned} \tag{2}$$

where the sums extend over the mode orders m, n. What remains is to determine the amplitudes f_m, b_m, u_n, d_n of the forward, backward, upward, and downward propagating fields. These are functions of the respective axis coordinate z of the horizontal waveguide (f_m, b_m) or x of the vertical core (u_n, d_n).

Note that the procedure outlined below applies to different structures as well, provided that it is possible to write down a reasonable field template in the form of Eq. (2), i.e. a superposition of known or conveniently computable fields with amplitudes that are each a function of a suitable propagation coordinate. If e.g. further (pieces of) x- or z-oriented waveguides are present, Eq. (2) would include summations over forward and backward modes associated with each horizontal channel, and summations over upward and downward modes of each vertical core, where the individual modes are included as far as physically reasonable.

2.2 Amplitude discretization

Next the amplitude functions are discretized using standard 1-D first order finite elements. We outline briefly the most simple version of an equidistant discretization for the function f_m. First an interval of arguments is identified outside of which the function can be assumed to be constant. In case of f_m this would be the horizontal extension $[z_0, z_N]$ of the computational window. Upon division of that interval in N equal pieces of length $\Delta z = (z_N - z_0)/N$, with nodal points $z_j = z_0 + j\,\Delta z$, one defines the piecewise linear element functions

$$\alpha_j(z) = \begin{cases} (z - z_{j-1})/\Delta z & \text{if } z_{j-1} \le z \le z_j, \\ (z_{j+1} - z)/\Delta z & \text{if } z_j \le z \le z_{j+1}, \\ 0 & \text{otherwise,} \end{cases} \qquad \text{for } j = 0, \ldots,\ N \tag{3}$$

with the exceptions that $\alpha_0(z) = 1$ if $z \leq z_0$, and $\alpha_N(z) = 1$ if $z_N \leq z$. For $j = 1, \ldots, N-1$ these are standard "triangle" functions; α_0 and α_N, the elements whose nodal points coincide with the boundaries of the computational interval, are 1 in the respective half-infinite exterior. f_m is expanded into the elements as

$$f_m(z) = \sum_{j=0}^{N} f_{m,j}\, \alpha_j(z)\,. \tag{4}$$

Observe that one of the coefficients $f_{m,j}$, here $f_{m,0}$, is actually a given quantity, representing the input amplitude of the mode of order m, prescribed at the left border of the computational window. All other values are so far unknown.

Analogous discretization procedures apply to b_m, u_n, and d_n. The coefficient functions are represented by discrete coefficients $b_{m,j}$, $u_{n,j}$, $d_{n,j}$, multiplied by element functions that in the last two cases depend on x. Also here values for the coefficients of the first elements, viewed along the respective direction of mode propagation, are given (zero, if only unidirectional influx along the horizontal channel is considered). After insertion of these expansions the ansatz (2) for the full electromagnetic field assumes the — abstract — form

$$\begin{pmatrix} \boldsymbol{E} \\ \boldsymbol{H} \end{pmatrix}(x,z) = \sum_k a_k\ \alpha_{\cdot}(\cdot)\, \boldsymbol{\psi}^{\cdot}_{\cdot}(x,z) =: \sum_k a_k \begin{pmatrix} \boldsymbol{E}_k \\ \boldsymbol{H}_k \end{pmatrix}(x,z). \tag{5}$$

Here the separate sums in Eqs. (2), (4) are merged into one summation over the formal index k that runs over waveguide channels, propagation directions, mode orders, and element numbers, indicated by the wildcards (dots) in the second term. It turns out to be convenient to combine the products of element functions α and mode fields $\boldsymbol{\psi}$ into "modal elements", functions of x and z, the quantities $(\boldsymbol{E}_k, \boldsymbol{H}_k)$ shown in the last term. The corresponding expansion coefficients $a_k \in \{f_{m,j}, b_{m,j}, u_{n,j}, d_{n,j}\}$ cover the unknowns and given values in the previous separate expansions.

2.3 Galerkin projection

The source-free frequency domain Maxwell equations for the electric field $\boldsymbol{E}$ and magnetic field $\boldsymbol{H}$ are to be solved within the computational domain:

$$\boldsymbol{\nabla} \times \boldsymbol{H} - \mathrm{i}\omega\epsilon_0\epsilon\boldsymbol{E} = 0\,, \qquad -\boldsymbol{\nabla} \times \boldsymbol{E} - \mathrm{i}\omega\mu_0\boldsymbol{H} = 0\,. \tag{6}$$

ϵ_0 and μ_0 are the vacuum permittivity and permeability; the dielectric permittivity $\epsilon(x,z) = n^2(x,z)$ includes the geometry and material properties of the structure under investigation.

Upon multiplying the first equation with the complex conjugate (*) of a trial field $\boldsymbol{E}'$, multiplying the second equation with the complex conjugate of a trial field $\boldsymbol{H}'$, adding the results, and integrating over the computational domain, one arrives at a weak form of Eqs. (6)

$$\iint \mathcal{K}(\boldsymbol{E}', \boldsymbol{H}'; \boldsymbol{E}, \boldsymbol{H})\, \mathrm{d}x\, \mathrm{d}z = 0 \tag{7}$$

with integrand

$$\mathcal{K}(\boldsymbol{E}', \boldsymbol{H}'; \boldsymbol{E}, \boldsymbol{H}) = (\boldsymbol{E}')^* \cdot (\boldsymbol{\nabla} \times \boldsymbol{H}) - (\boldsymbol{H}')^* \cdot (\boldsymbol{\nabla} \times \boldsymbol{E}) - \mathrm{i}\omega\epsilon_0\epsilon(\boldsymbol{E}')^* \cdot \boldsymbol{E} - \mathrm{i}\omega\mu_0(\boldsymbol{H}')^* \cdot \boldsymbol{H}\,. \tag{8}$$

For suitably smooth functions, the requirement that Eq. (7) holds for arbitrary trial fields $\boldsymbol{E}'$, $\boldsymbol{H}'$ guarantees that the fields $\boldsymbol{E}$, $\boldsymbol{H}$ satisfy Eqs. (6) inside the computational domain. No boundary terms appear in Eq. (7), hence no specific boundary conditions, other than those of the original space of functions, are enforced upon $\boldsymbol{E}$ and $\boldsymbol{H}$.

Obviously the integrand (8) vanishes locally (independent of the trial fields), if what is inserted for $\boldsymbol{E}$ and $\boldsymbol{H}$ solves Eqs. (6) exactly in the respective points. This can be relevant in the boundary regions when the CMT field template is used: in case of the waveguide crossing, the first and last modal elements of each channel consist of the modal fields, multiplied by element functions α that are constant outside the intervals $[z_0, z_N]$ or $[x_0, x_N]$, respectively. Outside the window $[z_0, z_N]$ or $[x_0, x_N]$ these are solutions of Eqs. (6). Hence the precise extension or shape of the integration domain in Eq. (7) (and consequently Eq. (9)) is irrelevant, as long as it covers the region with nonconstant element functions.

2.4 Numerical procedure

Now we proceed towards the numerical scheme along steps common for finite-element techniques. The CMT field template (5), in the abstract form $\boldsymbol{E} = \sum_k a_k \boldsymbol{E}_k$, $\boldsymbol{H} = \sum_k a_k \boldsymbol{H}_k$, replaces the target fields $\boldsymbol{E}$, $\boldsymbol{H}$ in Eq. (7). Then one abandons the constraint of vanishing Eq. (7) for arbitrary fields $\boldsymbol{E}'$, $\boldsymbol{H}'$, and restricts to the requirement that Eq. (7) should hold if a modal element $(\boldsymbol{E}_l, \boldsymbol{H}_l)$ is inserted for the trial fields, for all elements. Observing that the integrand (8) is bilinear in its two sets of electromagnetic field arguments, this leads to the set of algebraic equations

$$\sum_k K_{lk} a_k = 0, \quad \text{with} \quad K_{lk} = \iint \mathcal{K}(\boldsymbol{E}_l, \boldsymbol{H}_l; \boldsymbol{E}_k, \boldsymbol{H}_k)\, \mathrm{d}x\, \mathrm{d}z\,, \tag{9}$$

for all indices l of modal elements. In matrix form, with the coefficients a_k collected into a vector $\boldsymbol{a} = (\boldsymbol{u}, \boldsymbol{g})$ and ordered such that unknown $\boldsymbol{u}$ and given coefficients $\boldsymbol{g}$ are separated, and with the matrix elements K_{lk} arranged and split accordingly, Eq. (9) can be written

$$\begin{pmatrix} \mathsf{K}_{\mathrm{uu}} & \mathsf{K}_{\mathrm{ug}} \\ \mathsf{K}_{\mathrm{gu}} & \mathsf{K}_{\mathrm{gg}} \end{pmatrix} \begin{pmatrix} \boldsymbol{u} \\ \boldsymbol{g} \end{pmatrix} = 0\,, \quad \text{or} \quad \mathsf{K}_{\mathrm{u}} \boldsymbol{u} = -\mathsf{K}_{\mathrm{g}} \boldsymbol{g} \quad \text{with} \quad \mathsf{K}_{\mathrm{u}} = \begin{pmatrix} \mathsf{K}_{\mathrm{uu}} \\ \mathsf{K}_{\mathrm{gu}} \end{pmatrix}, \quad \mathsf{K}_{\mathrm{g}} = \begin{pmatrix} \mathsf{K}_{\mathrm{ug}} \\ \mathsf{K}_{\mathrm{gg}} \end{pmatrix}. \tag{10}$$

The matrix in the first system is square, thus the second system is overdetermined.[1] Hence we solve it in a least squares sense, i.e. the unknown coefficients $\boldsymbol{u}$ are computed as the solution of the system

$$\mathsf{K}_{\mathrm{u}}^{\dagger} \mathsf{K}_{\mathrm{u}} \boldsymbol{u} = -\mathsf{K}_{\mathrm{u}}^{\dagger} \mathsf{K}_{\mathrm{g}} \boldsymbol{g} \quad \text{or} \quad \boldsymbol{u} = -(\mathsf{K}_{\mathrm{u}}^{\dagger} \mathsf{K}_{\mathrm{u}})^{-1} \mathsf{K}_{\mathrm{u}}^{\dagger} \mathsf{K}_{\mathrm{g}} \boldsymbol{g}\,, \tag{11}$$

where the symbol † denotes the adjoint. In many cases the modal output amplitudes contained in $\boldsymbol{u}$ are already the most interesting results. The full HCMT solution for the optical field is obtained by inserting the values $\boldsymbol{u}$ and $\boldsymbol{g}$ for the coefficients in Eq. (5) or Eqs. (4), (2), respectively. Inspection of the respective amplitude functions (4) can then give an impression of the interaction of the coupled modes. While the above procedure may appear rather arbitrary, what concerns e.g. the steps from Eq. (6) to Eq. (7), or the choice of the trial fields in the numerical discretization, in the appendix we try to provide some motivation of why one proceeds as shown.

3 Examples

For a practical assessment of the HCMT approach, a series of 2-D examples is considered. A Helmholtz solver based on rigorous bi- or quadridirectional eigenmode expansions (BEP, QUEP) [12, 13, 14] is used as reference. The modesolver for 1-D multilayer slabs from [14] also provides the basis fields (1) for the HCMT implementation. What concerns the numerical effort, we like to emphasize that one actually solves a set of coupled 1-D equations, i.e. the size of the system Eq. (11) is small when compared to common 2-D or 3-D FE discretizations. Usually the assembly of the matrices, i.e. the evaluation of the integrals in Eq. (9), dominates the numerical effort, not the solution of Eq. (11).[2] The effort is thus determined by the number of modal basis elements, i.e. the number of channels, of (directonal) modes in each channel, and of the respective — not

[1] An alternative procedure could be considered: Eq. (7) is evaluated with the ansatz (5), now using only those modal elements as trial fields that correspond to *unknown* coefficients (or an arbitrary set of elements of the size of the number of unknowns). One arrives at a matrix equation like Eq. (10), now with a square matrix in the last equality. The least squares step can thus be avoided. We observed that procedure to converge as well; however, for finite stepsize the results appear less smooth and reasonable than what is obtained with the given recipe.

[2] Consequently, the least squares step leading to the system (11) does not impose a significant numerical burden, although any original sparsity of the system matrices is partly lost.

necessarily equal — FE stepsizes for the discretization of the amplitude functions. Further, structural properties in the form of overlaps of modal element domains have a strong influence: For the linear coupler of Section 3.2 each modal element is connected to only a few neighboring elements, leading to a mostly sparse matrix in Eq. (10). The connectivity is much higher for the crossed (pieces of) multimode channels in the resonator of Section 3.4. Here a larger fraction of nonzero integrals (9) have to be evaluated explicitly. Note that the assembly of the system matrices leaves much room for optimization e.g. in the form of avoiding redundant integrations, in particular if structural properties can be taken into account. Concerning accuracy, one should be aware that this is by construction an approximate method. With reduced FE stepsize the HCMT results are found to converge towards "continuous" approximations, which are as close to the exact solutions as permitted by the degrees of freedom in the respective field templates.

3.1 Straight waveguide

The straight waveguide of Figure 2 serves mainly to check for consistency, and to exclude alternative formulations concerning the algebraic procedure (cf. the remarks in the appendix). Here the CMT template consists merely of the fundamental forward propagating mode, with input amplitude $f_0 = 1$. The amplitude function is discretized by finite elements over the range $z \in [-20, 20]\,\mu$m with stepsize $\Delta z = 2\,\mu$m. The integrals (9) are evaluated on the computational window $z \in [< -20, > 20]\,\mu$m, $x \in [-3, 3]\,\mu$m that covers sufficiently the transverse mode profile extension.

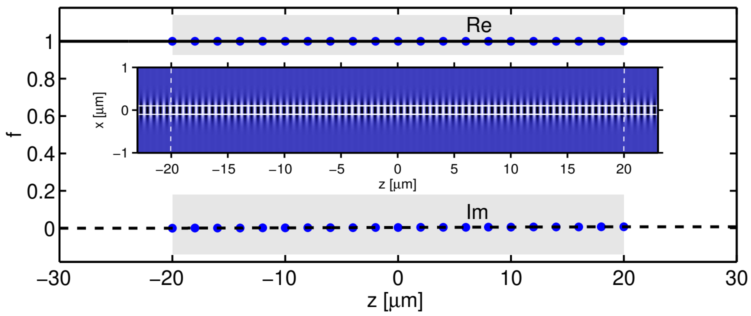

Figure 2: HCMT model of a symmetric straight singlemode slab (refractive indices 3.4 (core), 1.45 (cladding), thickness $0.2\,\mu$m), evolution of the single mode amplitude f with the coordinate z along the waveguide axis. Inset: snapshot of the optical field, the principal component E_y of the TE polarized wave at wavelength $\lambda = 1.55\,\mu$m is shown.

The procedure answers with the proper constant mode amplitude. The only thing worth noticing here is that the FE stepsize Δz is much larger than the wavelength of $0.57\,\mu$m associated with the modal field (actually 2 elements are sufficient). This emphasizes that in cases where one can expect the amplitude functions to change but slowly along their respective coordinates, only that slow variation needs to be resolved by the FE mesh, while the modal elements take care of the rapid oscillations in the optical fields.

3.2 Parallel cores

Figure 3 introduces a structure with two evanescently coupled parallel waveguide cores, the classical CMT problem. The fundamental forward propagating modes of the separate cores serve as basis fields, with an input amplitude $f_b = 1$ in the lower channel. The amplitude functions are allowed to vary over the interval $z \in [-20, 20]\,\mu$m of the FE mesh with a stepsize $\Delta z = 0.5\,\mu$m. Constant mode amplitudes violate Eqs. (6) outside that region, therefore here the computational window $z \in [-20, 20]\,\mu$m, $x \in [-3, 3]\,\mu$m has to be restricted to that longitudinal interval (in contrast to Section 3.1, cf. the remarks after Eq. (8)). The scheme adheres to the boundary conditions built into the field template, irrespectively of whether these are physical.

One observes the well known periodic coupling process, with a half beat length L_c that depends on all parameters of the structure. Figure 3(b) compares L_c, here viewed as a function of the coupler gap g, to the exact values (supermode analysis). Excellent agreement is found for wide gaps, with larger deviations for the less regular TM polarized fields. The plot also contains curves computed by a "conventional" CMT analysis, that are almost coinciding with the present data. Here the HCMT approach can be seen as the direct finite element solution of the ordinary differential equations (coupled mode equations) that emerge in common CMT formulations.

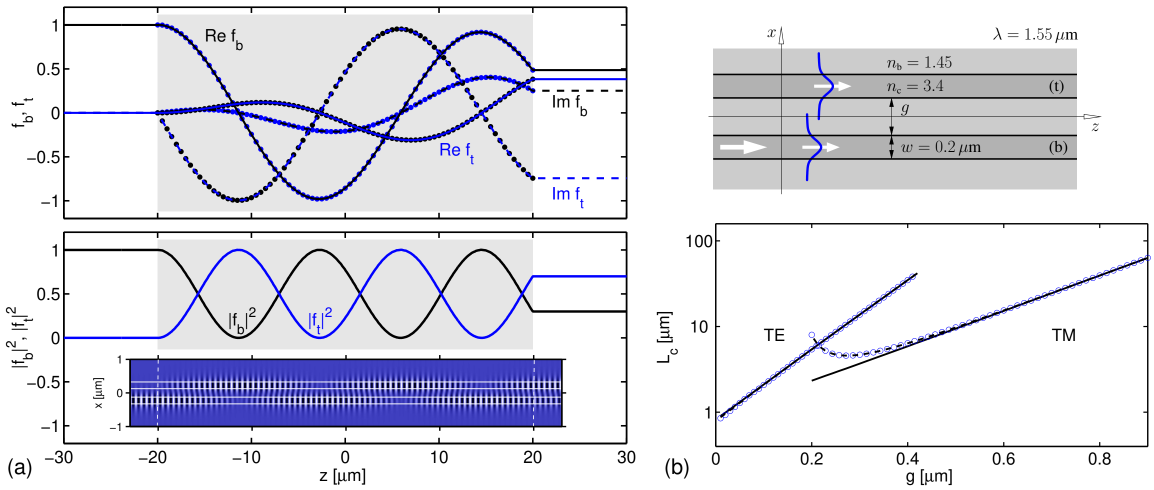

Figure 3: Two coupled parallel cores. (a), plots for a gap $g = 0.25\,\mu m$: amplitude functions of the basis modes, fields associated with the top (index t) and bottom cores (index b), real and imaginary parts (top) and absolute squares (bottom). The inset shows a time snapshot of the real, physical field. (b): coupling length L_c versus the gap width g. The continuous lines correspond to the exact length; circles denote the result of the present HCMT technique. Dashed lines (almost completely shadowed by the HCMT data, circles) are computed with a "conventional" CMT approach [1, 8].

3.3 Waveguide crossing

Figure 4 specifies parameters for the introductory example. Bidirectional variants of the guided modes of the horizontal and vertical cores constitute the CMT field template. The FE mesh covers the region $z \in [v/2 - 1.5\,\mu\text{m}, v/2 + 1.5\,\mu\text{m}]$, $x \in [w/2 - 1.5\,\mu\text{m}, w/2 + 1.5\,\mu\text{m}]$ with stepsizes $\Delta x = \Delta z = 0.025\,\mu$m. Integrals are evaluated over the computational window $x, z \in [-4, 4]\,\mu$m. Results for the crossing with vertical core width $v = 0.45\,\mu$m are summarized in Figure 4. Up to the missing radiative part, the HCMT field snapshot (b) covers nicely the guided wave features of the reference field (QUEP, (d)). Although here the viewpoint of coupled mode amplitude evolutions is not applicable, the technique still permits to inspect the amplitude functions (a)[3] (cf. Eq. (2)), as a means to illustrate the "coupling" of the basis fields, here e.g. in order to identify a central region of strong interaction.

For a more quantitative evaluation, Figure 5 shows the power transfer properties for crossings with different vertical core width v [13]. The periodic behaviour is attributed to newly supported guided modes in the vertical core with growing v. Given the simplicity of the field template, one observes a reasonable agreement with the QUEP reference results. With the present fine FE mesh, the HCMT scheme is power conservative on the scale of the figure (this criterion can serve as an indicator of convergence).

3.3.1 Radiated fields

According to plots (b) and (d) of Figure 4, the nonguided waves emerging radially from the center of the crossing form a major missing feature in the HCMT solution (Given the geometry of the structure, "physical intuition" could have roughly guessed this field form also without access to the reference solution: radiative waves originate from a localized source at the position where the waveguides perturb each other). As a — rather arbitrary — first attempt to cover these field parts with the present scheme, we add four Gaussian beams to the field template (2). The fields are outgoing along the four diagonals and focused at the four corner points $x = \pm w/2$, $z = \pm v/2$ with a waist of $0.5\,\mu$m. The beam shapes are multiplied by amplitude functions that depend on the diagonal distance from the corner, discretized by finite elements on a range of $1.5\,\mu$m with a stepsize of $0.025\,\mu$m.

The scheme adjusts the beam amplitudes such that the resulting field in Figure 4(c) resembles tolerably the reference data (d). The additional terms in the field template lower the total guided output power in Figure 5(b) to a level that is closer to the reference curves. This data already shows that any improvement effected by the

[3] The input amplitude $|f| = 1.0$ differs from 1 due to an overall phase adjustment to exhibit the maximum amplitude of the standing waves in the field plots Figure 4(b)–(d).

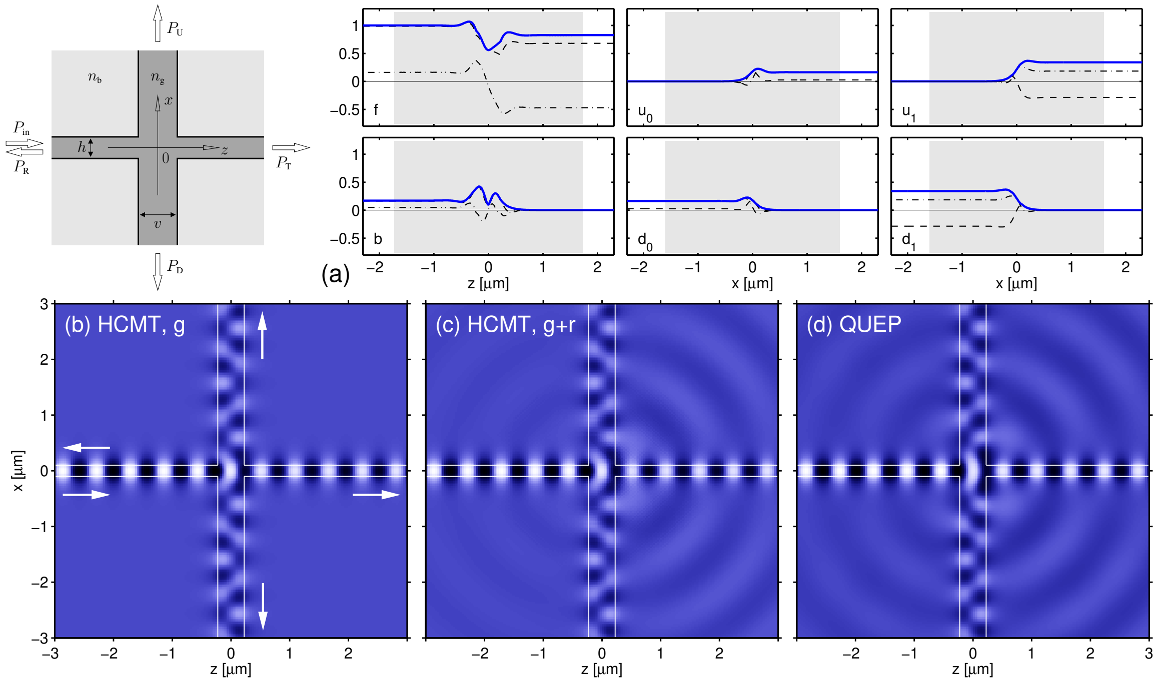

Figure 4: Waveguide crossing: A horizontal waveguide with thickness $h = 0.2\,\mu$m and refractive indices $n_g = 3.4$ (cores) and $n_b = 1.45$ (background) is crossed perpendicularly by a vertical core of variable width v. The propagation of TE polarized light at a vacuum wavelength $\lambda = 1.55\,\mu$m is considered. (a), HCMT simulation, $v = 0.45\,\mu$m: Amplitude functions f, b of the right- and left-traveling fundamental modes in the horizontal channel (first column), and functions u_n, d_n of the upward and downward propagating modes of order $n = 0, 1$ of the vertical channel (second and third columns); real parts (dashed), imaginary parts (dash-dotted), and absolute values (continuous lines) of the complex valued functions. Field plots, for $v = 0.45\,\mu$m: physical time snapshots of the principal component E_y of the TE fields as predicted by rigorous mode expansion simulations (QUEP, (d), reference [13]), by the HCMT procedure as outlined in Section 2 with guided modes used as basis fields (HCMT, g, (b)), and by a HCMT simulation where four Gaussian beams, oriented outward along the diagonals, have been used as additional basis fields (HCMT, g+r, (c), cf. Section 3.3.1).

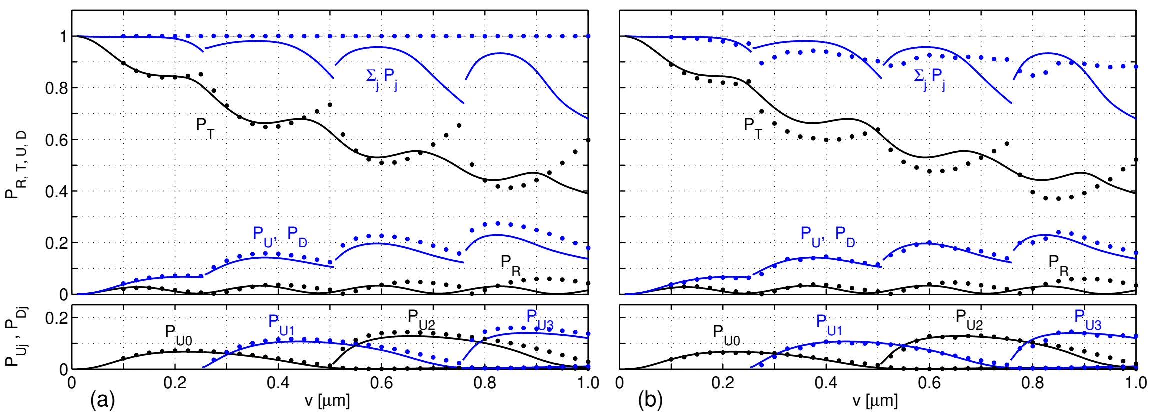

Figure 5: Guided power transmission through the waveguide crossing of Figure 4 versus the width v of the vertical core, HCMT results (dots) and QUEP simulations (lines, reference [13]). (a): HCMT simulations with only guided modes, (b): also Gaussian beams are included in the field template. For unit input in the left channel, P_R, P_T, P_U,and P_D are the relative power fractions carried by guided modes that leave the crossing along the left, right, upper, and lower channel. The top plots show also the sum of these quantities. Lower insets: power fractions $P_{Um} = P_{Dm}$ associated with guided modes of order $m = 0, 1, 2, 3$ of the multimode vertical channel.

presence of the Gaussians is strongly structure dependent. It is not at all evident that such a template would be useful in different regimes of parameters, e.g. for weaker refractive index contrast. Still, these — certainly not perfect — results show that, in cases where a plausible field template can be provided, the proposed technique can also cover radiative field contributions in a straightforward way.

3.4 Square resonator

Resonances of 2-D square cavities as the one in the structure of Figure 6 have been analyzed e.g. in Ref. [15]. A reasoning based on modal properties of 3-layer slab waveguides predicts that for the present cavity the 4th and 6th order modes of the symmetric slab with a thickness equal to the length W of the cavity edges play a dominant role. A HCMT simulation allows to verify that this also holds for the present structure with the access waveguides. Basis fields are here bidirectional versions of the single modes supported by the horizontal and vertical bus waveguides, and the 4th and 6th order modes of the slab of thickness W, where each field is included four times with the profiles rotated for propagation in the $\pm x$- and $\pm z$-directions. The amplitude functions are allowed to vary on respective intervals $x, z \in [-1.5, 1.5]\,\mu$m, discretized with a stepsize of $0.025\,\mu$m. All influx amplitudes are zero, with the exception of the mode coming in from the left in the lower bus core. Integrals are evaluated on the larger computational window $x, z \in [-4, 4]\,\mu$m.

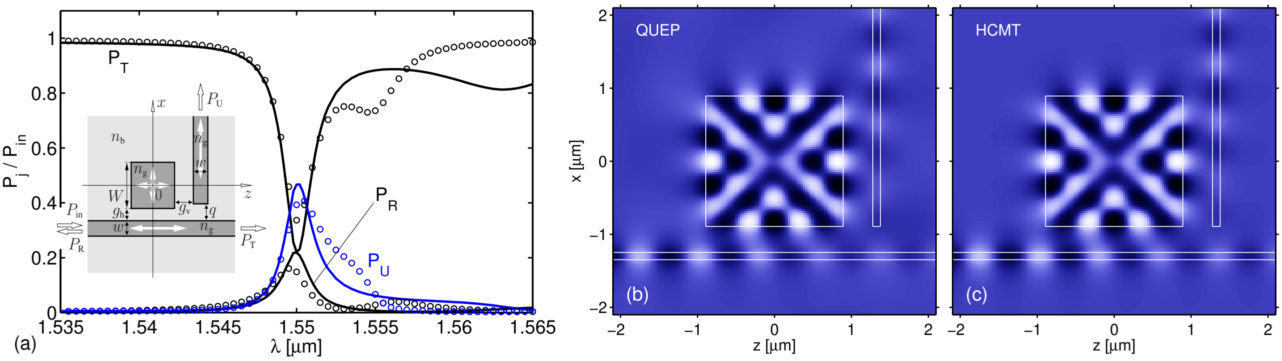

Figure 6: A square resonator with a perpendicular arrangement of access waveguides. Parameters, as introduced in the sketch: refractive indices $n_g = 3.4$ (guiding regions) and $n_b = 1.0$ (background), cavity side length $W = 1.786\,\mu$m, width of the waveguide cores $w = 0.1\,\mu$m, vertical gap $g_v = 0.385\,\mu$m, horizontal gap $g_h = q = 0.355\,\mu$m. The guided TE polarized mode of the horizontal channel is launched from the left. (a): Relative guided power fractions transfered to the right (transmitted, P_T), left (reflected, P_R), and upper exit port (P_U), HCMT results (dots) and QUEP reference (lines, [13]). (b), (c): time snapshots of the principal electric field component E_y at the resonance wavelength $\lambda = 1.55\,\mu$m, QUEP reference (b) and HCMT approximation (c).

According to Figure 6, the HCMT simulation resolves reasonably the resonance in question. This is confirmed also by the agreement in the snapshots of the resonant field profiles. The simplified HCMT model cannot account for all features of the transmission spectrum as e.g. near the right flank of the resonance peak, where other, guided and nonguided fields become relevant as well.

3.5 Waveguide Bragg grating-assisted rectangular resonator

From Ref. [16] we adopted a resonator concept and the related Bragg reflectors as examples for contradirectional coupled mode theory. The resonator (Figure 8) consists of a piece of a wide multimode waveguide that is terminated on both ends by Bragg gratings. Two parallel single-mode cores on both sides serve as bus waveguides. The Bragg gratings are tuned for highest reflectivity for the 5th order mode of the cavity slab. Likewise the modes of the bus waveguides are phase-matched to that field.

Figure 7 summarizes HCMT simulation for the Bragg reflectors. The field template comprises solely the 5th order mode of the slab of width W. The amplitude functions (functions of z) of its forward and backward versions are allowed to vary over the length of the grating corrugation. Since the amplitudes assume a staircase-like shape with steps located at the discontinuities of the grating teeth, here a nonequidistant discretization has been applied, with a nodal point at each refractive index step and the two neighboring ones by $0.02\,\mu$m apart. Where longer sections without refractive index steps are present in between, additional equidistant nodes were placed not further than $1\,\mu$m apart. Integrals were evaluated over the window $x \in [-7, 7]\,\mu$m, $z \in [0, 61.52]\,\mu$m. In Figure 7 one observes a quite satisfying agreement with the reference results.

The results of a HCMT simulation for the full resonator device are finally shown in Figure 8. Basis fields are bidirectional variants of the bus modes and of the 5th order mode of the cavity slab. The non-equidistant FE discretization covers the interval $z \in [101.513, 101.513]\,\mu$m, with a lateral computational window $x \in$

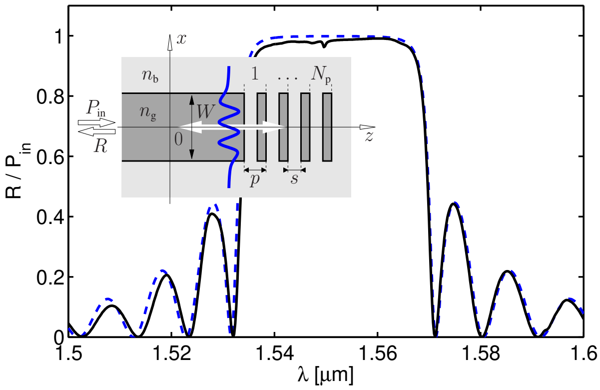

Figure 7: A waveguide Bragg reflector: the multimode waveguide (width $W = 9.955\,\mu m$, core refractive index $n_g = 1.6$, background $n_b = 1.45$) ends in a Bragg grating with $N_p = 40$ periods of length $p = 1.538\,\mu m$, with gaps of width $s = 0.281\,\mu m$. For a unit TE excitation of the 5-th order mode in the left half infinite part of the waveguide, the plot shows the relative power R reflected back into that mode, versus the vacuum wavelength λ. Continuous curve: rigorous calculations by bidirectional eigenmode propagation [12, 16], reference; dashed line: the present HCMT model.

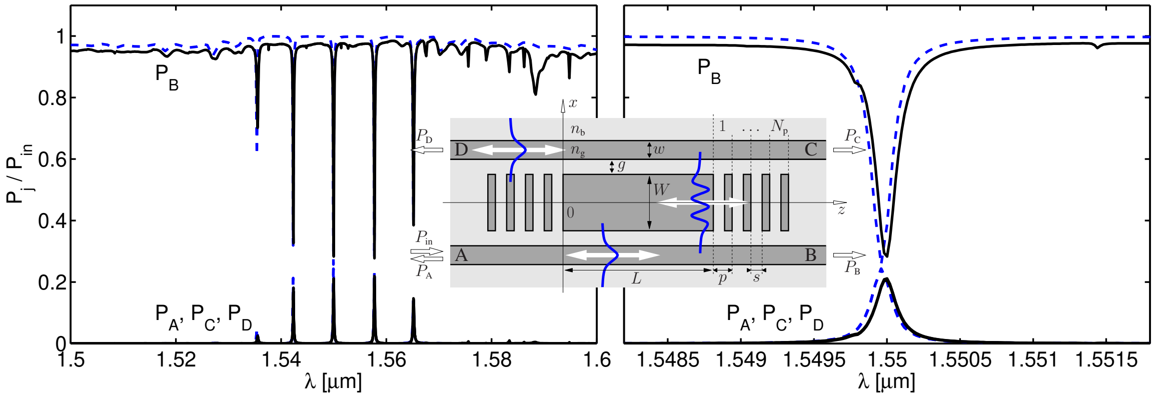

Figure 8: A Bragg-grating assisted resonator. Parameters are as introduced for Figure 7; the cavity of length $L = 79.985\,\mu m$ is coupled to bus waveguides of width $w = 1\,\mu m$, separated by gaps $g = 1.6\,\mu m$. The device is excited in port A by the fundamental, inward traveling TE mode of the lower core. Plots: relative power fractions P_B, and P_A, P_C, P_D (largely superimposed) transfered to the guided outward propagating modes in port B and in ports A, C, D, versus the vacuum wavelength λ; overview (left) and the region around one of the major resonances at $\lambda = 1.55\,\mu m$. Continuous line: simulations by bidirectional eigenmode propagation [12, 16], dashed curve: the present HCMT model.

$[-10, 10]\,\mu$m. While not all features of the reference spectrum are reproduced, the HCMT scheme captures the major resonances adequately.

Ref. [16] provides a an alternative coupled mode model for the resonator that combines separate solutions for codirectional propagation of evanescently coupled waves along the cavity segment $z \in [0, L]$ and for contradirectional wave interaction in the reflector gratings. There questions arise whether, for the computation of modal reflectivities and the net coupling effect along the cavity, the interaction between the outer channels and the central core needs to be taken into account also in the regions of the Bragg reflectors. Obviously the present approach avoids such questions by a homogeneous description of the full device.

4 Concluding remarks

In view of the field ansatz, the proposed approach may be regarded as a generalized ("hybrid", analytical/numerical) variant of coupled mode theory (HCMT), but one where the familiar viewpoint of mode amplitude evolutions along a common axis of propagation has to be abandoned. Still one can observe the evolution of the basis field amplitudes along their respective — possibly different — "natural" coordinates. Alternatively, this may be viewed as a numerical finite element technique with highly specialized, structure-adapted elements, consisting of the 1-D triangle functions that are used to discretize the amplitude functions, times the respective mode profiles (the "modal elements" introduced in Section 2.2). We have shown a series of benchmark-examples that allow to assess the performance and versatility of the method.

While so far only 2-D simulations have been carried out, the given formulation should permit a straightforward extension to 3-D. This concerns both the Galerkin procedure of Section 2 and the variational formulation outlined in the appendix. While for the 2-D simulations we could rely on analytical, i.e. for computational purposes exact, basis fields, these would have to be replaced by numerically computed mode profiles in the 3-D case. Here one should be aware that, although the variational derivation makes use of expansions into complete sets of modes on the respective port planes of the circuit, after the restriction to the CMT field templates only integrals over the few corresponding mode profiles at the port positions are required to evaluate the terms related to the transparent boundary conditions. Especially in 3-D simulations of this kind should constitute a viable alternative to rigorous "general purpose" numerical calculations, which frequently must be considered to be computationally prohibitively expensive.

With a "reasonable" trial field constituting the major ingredient, the entire approach necessarily relies to a large extent on physical / engineering intuition, i.e. on a thorough understanding of how the device in question actually works. As is the case with all CMT variants, beyond certain consistency checks (e.g. the power balance), there is usually no direct possibility for controlling the accuracy of the results for an unknown structure. Even for the given examples, there is no strict guarantee that the CMT model works properly in other regimes of parameters, e.g. for modified lengths/distances, wavelength, or polarization. Still, the examples of Section 3, including the parameter scans, show that the CMT templates indeed cover adequately some range of interesting structures. The present formalism then provides a straightforward way to quantify the intuitive models. Where possible (especially in 2-D, frequently not — or only with unacceptable numerical effort — in 3-D), benchmarking versus rigorous numerical simulations for characteristic configurations can give hints how far the approximate CMT model can be trusted, i.e. can provide a possibility to verify qualitatively and quantitatively the model assumptions.

A HCMT derived by variational restriction

A numerical scheme similar to the one of Section 2 can be derived on the basis of variational principles (cf. e.g. Ref. [1]). We choose the somewhat more abstract 3-D setting as introduced in Figure 9. Suppose the frequency domain Maxwell equations are to be solved inside the computational domain Ω, with a given, possibly inhomogeneous permittivity distribution within. Consider exemplarily a "port" plane S that is part of the boundary of Ω. The permittivity may be inhomogeneous around S. If it is, the inhomogeneity consists of waveguide cores with their axes oriented perpendicularly to S, i.e. the exterior of Ω beyond S and the immediate vicinity of S is z-homogeneous. The first step towards a variational formulation of the scattering problem is to identify suitable boundary conditions on S.

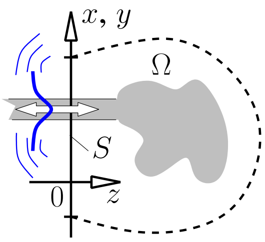

Figure 9: The region of interest, a domain Ω. The port plane S constitutes part of its boundary. A local coordinate system is placed such that the x and y axes span S, while the z-axis is oriented towards the interior of Ω.

A.1 Transparent influx boundary conditions for inhomogeneous exterior

To this end, we assume that a complete set of normal modes [1] associated with the cross-section S is available. Its elements are identified by a partly discrete and partly continuous "index" m; in the (practical) case that S is finite the set becomes discrete. Let the electric part $\tilde{\boldsymbol{E}}_m$ and the magnetic part $\tilde{\boldsymbol{H}}_m$ of the mode profiles, here functions of x and y, be chosen such that the combination $\tilde{\boldsymbol{\psi}}^{\mathrm{f}}_m = (\tilde{\boldsymbol{E}}_m, \tilde{\boldsymbol{H}}_m)$ represents waves that propagate in the positive z-direction towards the interior of Ω. For purposes of field expansions into these modes, one introduces the bilinear product

$$\langle \boldsymbol{A}, \boldsymbol{B} \rangle = \iint_S (\boldsymbol{A} \times \boldsymbol{B}) \cdot \boldsymbol{e}_z \, \mathrm{d}x \, \mathrm{d}y \tag{12}$$

for two fields $\boldsymbol{A}$, $\boldsymbol{B}$ on S, where $\boldsymbol{e}_z$ is the unit vector in the z-direction. The modes on S satisfy orthogonality properties with respect to this product in the form

$$\langle \tilde{\boldsymbol{E}}_l, \tilde{\boldsymbol{H}}_k \rangle = \delta_{lk} N_k \,, \quad \text{with nonzero} \quad N_k = \langle \tilde{\boldsymbol{E}}_k, \tilde{\boldsymbol{H}}_k \rangle \,, \tag{13}$$

with $\delta_{lk} = 1$, if $l = k$, otherwise $\delta_{lk} = 0$. The mode set is complete in the sense that "any" [1] electric field $\boldsymbol{E}$ and magnetic field $\boldsymbol{H}$ on S can be expanded as

$$\boldsymbol{E} = \sum_m e_m \tilde{\boldsymbol{E}}_m \quad \text{and} \quad \boldsymbol{H} = \sum_m h_m \tilde{\boldsymbol{H}}_m \tag{14}$$

with coefficients $e_m = \langle \boldsymbol{E}, \tilde{\boldsymbol{H}}_m \rangle / N_m,\ h_m = \langle \tilde{\boldsymbol{E}}_m, \boldsymbol{H} \rangle / N_m$. One should be aware that the notions introduced rather sloppily above are formal e.g. with respect to the ranges of summation / integration (index m), or with respect to the completeness, where the product (12) touches only the transverse x- and y-components of the supplied fields, i.e. also the expansions concern only these transverse components. This is however sufficient for the purposes below.

The boundary conditions on S have to distinguish inward and outward traveling fields. It is therefore convenient to observe that a field on S with arbitrary electric and magnetic part can be expanded into modes traveling forward and backward along the z-axis:

$$\begin{pmatrix} \boldsymbol{E} \\ \boldsymbol{H} \end{pmatrix} = \sum_m f_m \begin{pmatrix} \tilde{\boldsymbol{E}}_m \\ \tilde{\boldsymbol{H}}_m \end{pmatrix} + \sum_m b_m \begin{pmatrix} \tilde{\boldsymbol{E}}_m \\ -\tilde{\boldsymbol{H}}_m \end{pmatrix} . \tag{15}$$

Here the combination $\tilde{\boldsymbol{\psi}}_m^{\mathrm{b}} = (\tilde{\boldsymbol{E}}_m, -\tilde{\boldsymbol{H}}_m)$ is the backward propagating version of $\tilde{\boldsymbol{\psi}}_m^{\mathrm{f}}$, where as before the equations are formal in that they concern only transverse components. Given the coefficients e_m, h_m of individual expansions (14) for the electric and magnetic parts, the coefficients in Eq. (15) are $f_m = (e_m + h_m)/2$ and $b_m = (e_m - h_m)/2$.

Using these formal ingredients, we can now state transparent influx boundary conditions (TIBCs) on the port plane S. These conditions should allow to specify optical influx across S into Ω, while waves from inside Ω are permitted to pass through S towards the exterior. In view of the expansion (15), they should prescribe given values F_m for the amplitudes f_m of the modes traveling into Ω, while no restrictions are placed on the amplitudes b_m of the waves traveling outward.[4] This is achieved by requiring the solution $\boldsymbol{E}$, $\boldsymbol{H}$ of the problem in Ω to satisfy the following expressions on S (transverse components only):

$$\boldsymbol{E} = \sum_m 2F_m \tilde{\boldsymbol{E}}_m - \sum_m \frac{1}{N_m} \langle \tilde{\boldsymbol{E}}_m, \boldsymbol{H} \rangle \tilde{\boldsymbol{E}}_m \,, \quad \boldsymbol{H} = \sum_m 2F_m \tilde{\boldsymbol{H}}_m - \sum_m \frac{1}{N_m} \langle \boldsymbol{E}, \tilde{\boldsymbol{H}}_m \rangle \tilde{\boldsymbol{H}}_m \,. \tag{16}$$

By inserting the expansion Eq. (15), it is straightforward to show that both parts of Eqs. (16) fix the inward amplitudes to the proper values $f_m = F_m$, while the coefficients b_m drop from the equations, i.e. are not restricted by the boundary conditions.

A.2 Variational form of the scattering problem

Consider the following functional of the six electromagnetic field components

$$\begin{aligned} \mathcal{F}(\boldsymbol{E}, \boldsymbol{H}) \;=\; & \iiint_\Omega \left\{ \boldsymbol{E} \cdot (\boldsymbol{\nabla} \times \boldsymbol{H}) + \boldsymbol{H} \cdot (\boldsymbol{\nabla} \times \boldsymbol{E}) - \mathrm{i}\omega\epsilon_0\epsilon \boldsymbol{E}^2 + \mathrm{i}\omega\mu_0 \boldsymbol{H}^2 \right\} \mathrm{d}x\, \mathrm{d}y\, \mathrm{d}z \\ & - \sum_m 2F_m \left\{ \langle \tilde{\boldsymbol{E}}_m, \boldsymbol{H} \rangle - \langle \boldsymbol{E}, \tilde{\boldsymbol{H}}_m \rangle \right\} + \sum_m \frac{1}{2N_m} \left\{ \langle \tilde{\boldsymbol{E}}_m, \boldsymbol{H} \rangle^2 - \langle \boldsymbol{E}, \tilde{\boldsymbol{H}}_m \rangle^2 \right\} \end{aligned} \tag{17}$$

which is equivalent to an expression in [1] (Eqn. (1.97)), apart from the boundary integrals. $\mathcal{F}$ can be seen as a generalization / adaption of the variational formulations for 1-D / 2-D second order systems (scalar Helmholtz

[4] For influx prescribed in the form of given electromagnetic field components, i.e. a field of the form $(\boldsymbol{E}_{\text{in}}, \boldsymbol{H}_{\text{in}}) = \sum_m F_m \tilde{\boldsymbol{\psi}}_m^{\mathrm{f}}$, the first sums in Eqs. (16) reduce to the terms $2\boldsymbol{E}_{\text{in}}$ and $2\boldsymbol{H}_{\text{in}}$. The same holds for the corresponding terms in the functional (17).

equation with TIBCs) of Refs. [10] / [11] to the present 3-D (2-D) vectorial first order problems with inhomogeneous exterior, i.e. with incoming waveguides.

Using the rules of variational and vector calculus, one readily shows that the first variation of $\mathcal{F}$ is

$$\begin{aligned}
\delta\mathcal{F}(\boldsymbol{E},\boldsymbol{H};\delta\boldsymbol{E},\delta\boldsymbol{H}) &= \iiint_\Omega \{2\delta\boldsymbol{E}\cdot(\boldsymbol{\nabla}\times\boldsymbol{H}-\mathrm{i}\omega\epsilon_0\epsilon\boldsymbol{E})+2\delta\boldsymbol{H}\cdot(\boldsymbol{\nabla}\times\boldsymbol{E}+\mathrm{i}\omega\mu_0\boldsymbol{H})\}\,\mathrm{d}x\,\mathrm{d}y\,\mathrm{d}z \\
&+ \langle \boldsymbol{E}-\sum_m 2F_m\tilde{\boldsymbol{E}}_m+\sum_m\frac{1}{N_m}\langle\tilde{\boldsymbol{E}}_m,\boldsymbol{H}\rangle\tilde{\boldsymbol{E}}_m,\,\delta\boldsymbol{H}\rangle \\
&- \langle \delta\boldsymbol{E},\,\boldsymbol{H}-\sum_m 2F_m\tilde{\boldsymbol{H}}_m+\sum_m\frac{1}{N_m}\langle\boldsymbol{E},\tilde{\boldsymbol{H}}_m\rangle\tilde{\boldsymbol{H}}_m\rangle \\
&- \iint_{\partial\Omega\backslash S}\{(\boldsymbol{n}\times\boldsymbol{E})\cdot\delta\boldsymbol{H}+(\boldsymbol{n}\times\boldsymbol{H})\cdot\delta\boldsymbol{E}\}\,\mathrm{d}A\,.
\end{aligned} \tag{18}$$

Here $\boldsymbol{n}\mathrm{d}A$ indicates outward oriented surface elements on $\partial\Omega$. If $\mathcal{F}$ becomes stationary for fields $\boldsymbol{E}$, $\boldsymbol{H}$, i.e. if the first variation (18) vanishes for arbitrary $\delta\boldsymbol{E}$, $\delta\boldsymbol{H}$, then $\boldsymbol{E}$ and $\boldsymbol{H}$ satisfy Eqs. (6) in Ω, they satisfy the TIBCs (16) on S (the terms with the product (12) cover the boundary integrals over S), and the transverse components of both $\boldsymbol{E}$ and $\boldsymbol{H}$ vanish on all other parts $\partial\Omega\backslash S$ of the boundary.

In case a domain with more input/output ports is considered, with TIBCs on each port plane, the functional (17) would have to be extended by boundary terms in a completely analogous way. For the waveguide crossing of Section 2, Ω would be the computational window as introduced in Figure 1; its edges would act as four port planes (lines in 2-D).

A.3 Variational HCMT scheme

Upon insertion of the field ansatz (5), $\mathcal{F}$ becomes a function of the coefficients $\boldsymbol{a}=(\dots,a_k,\dots)$ of all modal elements. The function is quadratic in these unknowns, with an additional linear term,

$$\mathcal{F}_\mathrm{r}(\boldsymbol{a})=\sum_{l,k}a_la_kF_{lk}+\sum_l a_lR_l+\sum_{l,k}a_la_kB_{lk}=\boldsymbol{a}\cdot\mathsf{F}\boldsymbol{a}+\boldsymbol{R}\cdot\boldsymbol{a}+\boldsymbol{a}\cdot\mathsf{B}\boldsymbol{a}\,, \tag{19}$$

where the entries F_{lk}, R_l, and B_{lk} of the matrices / the vector F, $\boldsymbol{R}$ and B are

$$F_{lk}=\iiint_\Omega\{\boldsymbol{E}_l\cdot(\boldsymbol{\nabla}\times\boldsymbol{H}_k)+\boldsymbol{H}_l\cdot(\boldsymbol{\nabla}\times\boldsymbol{E}_k)-\mathrm{i}\omega\epsilon_0\epsilon\boldsymbol{E}_l\cdot\boldsymbol{E}_k+\mathrm{i}\omega\mu_0\boldsymbol{H}_l\cdot\boldsymbol{H}_k\}\,\mathrm{d}x\,\mathrm{d}y\,\mathrm{d}z\,, \tag{20}$$

$$R_l=-\sum_m 2F_m\left\{\langle\tilde{\boldsymbol{E}}_m,\boldsymbol{H}_l\rangle-\langle\boldsymbol{E}_l,\tilde{\boldsymbol{H}}_m\rangle\right\}\,, \tag{21}$$

$$B_{lk}=\sum_m\frac{1}{2N_m}\left\{\langle\tilde{\boldsymbol{E}}_m,\boldsymbol{H}_l\rangle\langle\tilde{\boldsymbol{E}}_m,\boldsymbol{H}_k\rangle-\langle\boldsymbol{E}_l,\tilde{\boldsymbol{H}}_m\rangle\langle\boldsymbol{E}_k,\tilde{\boldsymbol{H}}_m\rangle\right\}\,. \tag{22}$$

Further contributions to R_l and B_{lk} occur, if more port planes are present in the actual problem.

In order to identify an optimum approximation to the problem of Section A.2, given the restricted space of functions provided by the field template (5), one now looks for vectors $\boldsymbol{a}$ where the restricted functional (19) becomes stationary. The first variation of $\mathcal{F}_\mathrm{r}$,

$$\delta\mathcal{F}_\mathrm{r}=\delta\boldsymbol{a}\cdot\left(\left((\mathsf{F}+\mathsf{B})+(\mathsf{F}+\mathsf{B})^\mathsf{T}\right)\boldsymbol{a}+\boldsymbol{R}\right)\,, \tag{23}$$

is required to vanish for arbitrary variations $\delta\boldsymbol{a}$. The optimum vector of coefficients is thus given by the solution of the linear system

$$\mathsf{M}\boldsymbol{a}+\boldsymbol{R}=0\,,\quad\text{with}\quad\mathsf{M}=\left((\mathsf{F}+\mathsf{B})+(\mathsf{F}+\mathsf{B})^\mathsf{T}\right)\,. \tag{24}$$

One could directly use the result of Eq. (24) to assemble the CMT field. In that case the error necessarily introduced by the use of the CMT template will be distributed over all coefficients, also those that represent the given influx, i.e. those for which values are actually known (f_m will slightly deviate from F_m, cf. Section A.1). We therefore propose to view Eq. (24) as an overdetermined system for the unknowns $\boldsymbol{u}$, in $\boldsymbol{a} = (\boldsymbol{u}, \boldsymbol{g})$, where $\boldsymbol{g}$ are the given, influx-related values, and then to solve the system for $\boldsymbol{u}$ in a least squares sense. This also turns out to be beneficial for the smoothness of the results. Upon splitting M and $\boldsymbol{R}$ according to $\boldsymbol{a}$, Eq. (24) reads

$$\begin{pmatrix} \mathsf{M}_{\mathrm{uu}} & \mathsf{M}_{\mathrm{ug}} \\ \mathsf{M}_{\mathrm{gu}} & \mathsf{M}_{\mathrm{gg}} \end{pmatrix} \begin{pmatrix} \boldsymbol{u} \\ \boldsymbol{g} \end{pmatrix} = - \begin{pmatrix} \boldsymbol{R}_{\mathrm{u}} \\ \boldsymbol{R}_{\mathrm{g}} \end{pmatrix}, \quad \text{or} \quad \mathsf{M}_{\mathrm{u}} \boldsymbol{u} = -\boldsymbol{h} \quad \text{with} \quad \mathsf{M}_{\mathrm{u}} = \begin{pmatrix} \mathsf{M}_{\mathrm{uu}} \\ \mathsf{M}_{\mathrm{gu}} \end{pmatrix}, \quad \boldsymbol{h} = \begin{pmatrix} \boldsymbol{R}_{\mathrm{u}} \\ \boldsymbol{R}_{\mathrm{g}} \end{pmatrix} + \begin{pmatrix} \mathsf{M}_{\mathrm{ug}} \\ \mathsf{M}_{\mathrm{gg}} \end{pmatrix} \boldsymbol{g}, \tag{25}$$

and the actual unknowns $\boldsymbol{u}$ are found as the solution of the equation

$$\mathsf{M}_{\mathrm{u}}^{\dagger} \mathsf{M}_{\mathrm{u}} \boldsymbol{u} = -\mathsf{M}_{\mathrm{u}}^{\dagger} \boldsymbol{h}. \tag{26}$$

Modal output amplitudes are already included in these unknowns; the full CMT field can be assembled by evaluating Eq. (5) with the coefficients $\boldsymbol{a} = (\boldsymbol{u}, \boldsymbol{g})$.

A.4 Comments

Comparison of Eqs. (8)–(11) with (20)–(22), (24)–(26) reveals that, with the exception of the boundary terms, the implementation of the scheme just derived requires only minor changes with respect to Section 2. For e.g. the waveguide crossing of Section 3.3, with the field ansatz and the FE discretization as before, the procedure of Section A.3 leads to results that are indistinguishable from the data shown in Figure 5.

What concerns the boundary integrals in Eqs. (21), (22), note that only those few modal elements with nonzero field values at the port planes contribute to the TIBC-related terms R_l, B_{lk}. Still, at a first glance it may seem as if complete (or large truncated) sets of normal modes are required at each port plane to evaluate these terms, which would impose a serious numerical burden in case of 3-D simulations. In at least two practical situations, however, it turns out that this difficulty can be avoided. If, as for the waveguide crossing, the relevant modal elements consist of mode profiles that are part of the local expansion basis, only the terms related to that particular mode remain in Eqs. (21), (22), while all others vanish due to the orthogonality properties (13). If, as for e.g. the case of the Gaussian beams used to represent radiation in the example of Section 3.3.1, only two elements, the bidirectional versions of the same field, are present at the port plane (where the input amplitudes F_m are previously being determined by expanding that field into the local mode set), the integrals in Eqs. (21), (22) reduce to products (12) of the respective trial field itself. There are, however, structures that can not be covered without a more rigorous expansion at the boundary. An example is the waveguide coupler, when being modeled using the modes of the individual channels in the field template, as in Section 3.2. Clearly, here the modal expansion on the port planes needs to include at least the fundamental symmetric and antisymmetric supermodes of the full structure (the computation of which is what one likes to avoid when using CMT) to provide transparent boundary conditions.

A more serious limitation of the functional (17), when applied for purposes of a CMT-like approximation, is that it needs bidirectional versions of modal elements to be present in the field template. Corresponding remarks can be found in Ref. [1]. This limitation transfers to the numerical scheme of Section A.3: Inspection of e.g. the expression (21) for the boundary term containing the influx amplitudes shows that R_l vanishes, if modal element l corresponds to a forward (inward propagating) mode, while there is a nonzero contribution with the given coefficient F_k if a modal element k represents the related backward wave. Consequently, the scheme requires forward and backward waves for all channels to be included in the field template. Simulations like in Sections 3.1, 3.2 with only unidirectional field templates fail with the scheme above. Therefore, in cases where both schemes are applicable the (simpler) one of Section 2 seems preferable.

Finally note that Eq. (7) is related to the functional [1] (Eqn. (1.98))

$$\mathcal{C}(\boldsymbol{E}, \boldsymbol{H}) = \iiint_{\Omega} \{ \boldsymbol{E}^* \cdot (\boldsymbol{\nabla} \times \boldsymbol{H}) - \boldsymbol{H}^* \cdot (\boldsymbol{\nabla} \times \boldsymbol{E}) - \mathrm{i}\omega\epsilon_0\epsilon \boldsymbol{E}^* \cdot \boldsymbol{E} + \mathrm{i}\omega\mu_0 \boldsymbol{H}^* \cdot \boldsymbol{H} \} \, \mathrm{d}x \, \mathrm{d}y \, \mathrm{d}z \,. \tag{27}$$

Just as for $\mathcal{F}$, stationarity of $\mathcal{C}$ guarantees that its arguments $\boldsymbol{E}$ and $\boldsymbol{H}$ satisfy Eqs. (6) in the domain Ω. Up to boundary terms the first variation of $\mathcal{C}$ is identical to Eq. (7), with the variations $\delta\boldsymbol{E}$, $\delta\boldsymbol{H}$ replacing the trial fields

$\boldsymbol{E}'$, $\boldsymbol{H}'$. The boundary terms $-\iint_{\partial\Omega}\{(\boldsymbol{n}\times\boldsymbol{E}^*)\cdot\delta\boldsymbol{H}-(\boldsymbol{n}\times\boldsymbol{H}^*)\cdot\delta\boldsymbol{E}\}\,\mathrm{d}A$ in $\delta\mathcal{C}$ (cf. Section A.2), however, imply natural boundary conditions of vanishing transverse components of $\boldsymbol{E}$ and $\boldsymbol{H}$ on $\partial\Omega$. If $\mathcal{C}$ could be extended by boundary integrals such that the boundary terms in $\delta\mathcal{C}$ cancel, then the scheme of Section 2 could be seen as a restriction of $\mathcal{C}$ to the CMT template (5).[5]

Acknowledgments

This work has been supported by the Dutch Technology foundation (BSIK / NanoNed project TOE.7143). The author thanks E. van Groesen, H. J. W. M. Hoekstra, A. Sopaheluwakan, and R. Stoffer for many fruitful discussions.

References

[1] C. Vassallo. *Optical Waveguide Concepts*. Elsevier, Amsterdam, 1991.

[2] W. P. Huang. Coupled mode theory for optical waveguides: an overview. *Journal of the Optical Society of America A*, 11(3):963–983, 1994.

[3] D. G. Hall and B. J. Thompson, editors. *Selected Papers on Coupled-Mode Theory in Guided-Wave Optics*, volume MS 84 of *SPIE Milestone Series*. SPIE Optical Engineering Press, Bellingham, Washington USA, 1993.

[4] S. L. Chuang. A coupled mode formulation by reciprocity and a variational principle. *Journal of Lightwave Technology*, 5(1):5–15, 1987.

[5] D. R. Rowland and J. D. Love. Evanescent wave coupling of whispering gallery modes of a dielectric cylinder. *IEE Proceedings, Pt. J*, 140(3):177–188, 1993.

[6] K. R. Hiremath, R. Stoffer, and M. Hammer. Modeling of circular integrated optical microresonators by 2-D frequency-domain coupled mode theory. *Optics Communications*, 257(2):277–297, 2006.

[7] R. Stoffer, K. R. Hiremath, M. Hammer, L. Prkna, and J. Čtyroký. Cylindrical integrated optical microresonators: Modeling by 3-D vectorial frequency domain coupled mode theory. *Optics Communications*, 256(1–3):46–67, 2005.

[8] M. Lohmeyer, N. Bahlmann, O. Zhuromskyy, and P. Hertel. Radiatively coupled waveguide polarization splitter simulated by wave-matching based coupled mode theory. *Optical and Quantum Electronics*, 31:877–891, 1999.

[9] J. B. Nicolau and E. van Groesen. Hybrid analytical-numeric method for light through a bounded planar dielectric structure. *Journal of Nonlinear Optical Physics and Materials*, 14(2):161–176, 2005.

[10] E. W. C. van Groesen and J. Molenaar. *Continuum Modeling in the Physical Sciences*. SIAM publishers, March 2007 (to appear).

[11] A. Sopaheluwakan. *Characterization and Simulation of Localized States in Optical Structures*. University of Twente, Enschede, The Netherlands, 2006. Ph.D. Thesis.

[12] M. Lohmeyer and R. Stoffer. Integrated optical cross strip polarizer concept. *Optical and Quantum Electronics*, 33(4/5):413–431, 2001.

[13] M. Hammer. Quadridirectional eigenmode expansion scheme for 2-D modeling of wave propagation in integrated optics. *Optics Communications*, 235(4–6):285–303, 2004.

[14] M. Hammer. METRIC — Mode expansion tools for 2D rectangular integrated optical circuits. http://www.math.utwente.nl/∼hammerm/Metric/.

[15] M. Hammer. Resonant coupling of dielectric optical waveguides via rectangular microcavities: The coupled guided mode perspective. *Optics Communications*, 214(1–6):155–170, 2002.

[16] M. Hammer, D. Yudistira, and R. Stoffer. Modeling of grating assisted standing wave microresonators for filter applications in integrated optics. *Optical and Quantum Electronics*, 36(1–3):25–42, 2004.

[5] Likewise, for a domain enclosed by input/output ports, an extension of $\mathcal{C}$ by terms as in $\mathcal{F}$ (then using a product [1] with complex conjugated fields, or even a symmetrized version that distinguishes forward and backward waves [12]) would be desirable, that leads to TIBCs as natural boundary conditions.